Parametric Design Studies of the Helicopter Rotor Noise using Variable-Fidelity Methods

Dirk Rabe **Gunther Wilke**
German Aerospace Center (DLR)
Braunschweig, Germany

ABSTRACT

The current trend is to produce even quieter helicopters in order to increase public acceptance. While the ERATO and the from it evolved Blue Edge® blade show that noise reduction can be achieved through a specific blade design; the task to arrive at such a design is lengthy. It roughly took 25 years from the wind tunnel campaign to the now flying H160 with this type of rotor design. In order to speed up the design process, it is necessary to quickly and accurately assess the quality of a given design. While a wide range of tools exists to predict rotorcraft noise, the validity as well as the accuracy per computational cost has not been fully evaluated. Recent CFD simulations are able to replicate the BVI noise event, yet are very costly in contrast to wake coupled comprehensive codes. This paper seeks the best method that fulfills the trade-off between speed and accuracy. Therefore, three different rotor wind tunnel models in descent flight are computed with six different methods. Afterwards, a selection of these methods is utilized in a parametric study to further see how well the different methods can identify the best blade design. The most favored method is a panel method coupled with a free wake model including structural modelling from a comprehensive code, while CFD is recommended only to check the final design due to its high computational cost.

NOMENCLATURE

a_∞	speed of sound in m/s
c	chord length in m
$c_n M^2$	section normal force coefficient $(2n)/(\rho_\infty a_\infty^2 c(r)dr)$
$dc_n M^2/d\psi$	derivative of section normal force coefficient in $-/^o$
c_T	thrust coefficient $T/(\rho \Pi R^2 a_\infty^2 M_{tip}^2)$
dr	radial integrand in m
M_∞	free-stream Mach number
M_{tip}	Blade tip mach number
n/dr	section nomral force in N/m
N_b	number of blades
R	blade radius in m
RPM	(rotor) rounds per minute
T	rotor thrust
α_c	corrected shaft angle
μ	advance ratio M_∞/M_{tip}
ρ_∞	density of air kg/m^3
ψ	rotor azimuth location in ^{o}
σ	rotor solidity $N_b c/(\Pi R^2)$
$\theta_{0,c,s}$	collective, lateral and longitudinal pitch control angles

INTRODUCTION

The utility of a helicopter is without question: Its specialty is hovering flight, which allows it to take-off and land vertically and perform tasks that regular fixed-wing aircraft cannot. However, in contrast to fixed-wing aircraft, noise is of greater concern, since helicopters operate in low-altitude (urban) environments, which makes the helicopter a greater annoyance for the general public. In particular during descent flight, the helicopter generates a significant amount of noise from the interaction of the rotor blades with its own wake and vortices as the helicopter sinks through them. This effect is known as blade-vortex-interaction (BVI).

A lot of effort has been put into reducing the BVI noise of the helicopter. On the one hand, noise abatement flight procedures are developed at DLR (Ref. 1), which try to avoid the noise reaching the public by altering the flight path. On the other hand, there is the route of actively controlling the rotor blade motion to reduce the noise generation in the first place. The renowned wind tunnel campaign HARTII (Ref. 2) investigates the effect of higher harmonic controls (HHC) for helicopter rotor blades. They reduce noise or vibration noticeably by employing HHC to the model scale BO-105 rotor. A last option exists for reducing the rotor noise, which is reshaping the blade so that it produces less noise. A good example is the ERATO rotor, with an overview given by van der Wall et al. (Ref. 3). The ERATO blade is an advanced double-swept blade design, which has been tested in a wind tunnel campaign along with the 7AD rotor blade. It has been developed into the Blue Edge® blade know flying the Airbus Helicopters H160 model (Ref. 3).

In order to design such a blade, a lot of knowledge of the flow physics in which the blade operates is necessary. While for the ERATO blade, the blade element theory (BET) coupled with either a prescribed wake model in DLR's S4 according to Bed-

Presented at the AHS International 74th Annual Forum & Technology Display, Phoenix, Arizona, USA, May 14–17, 2018.

does (Ref. 4) or the free wake model MESIR (Ref. 5) in the R85 code (Ref. 6) on the French side have been used, today's simulation toolbox has grown substantially. Boyd (Ref. 7) accurately captures the BVI phenomenon with computational fluid dynamics (CFD) and reproduces the HART II noise carpets well. Later, Smith et al. (Ref. 8) compare various CFD methods. Many of these are readily able to predict the force fluctuations caused by the BVI phenomenon. Jain et al. improve their HART II results to the point that the vortex trajectories are matched well with the experiment by increasing the order of their numerical methods as well as apply mesh refinement (Ref. 9). Wilke (Ref. 10) utilizes an efficient higher order scheme to arrive at plausible results with a fair amount of grid points. While these examples have yielded good results for the HART II rotor, Kowarsch et al. (Ref. 11) are able to replicate flight test data of an EC135 helicopter with their CFD method.

While these advances in CFD demonstrate that the BVI noise can be correctly predicted, it is still uncertain if CFD should be employed in an industrial context due to its great resource demands. Generating computational meshes for higher order schemes and then solving the Reynolds-average Navier-Stokes (RANS) equations on multi-million point meshes is still a time demanding task despite the vast available computer power. Recently, Yin et al. (Ref. 12) show promising results using a panel method coupled to a free-wake model. This approach poses and intermediate simulation tool in between comprehensive codes coupled with a wake model and full blown CFD.

Going back to the ERATO rotor, from the initial wind tunnel model to the flying product, the Blue Edge® blade, roughly a quarter century has passed. The question is, can better blades be obtained in faster turnaround times with the larger choice of tools available? In this paper, methods ranging from the BET coupled with prescribed wake models to panel methods up to CFD with higher order schemes are tried to examine how well they can predict the noise carpets of different rotor geometries. First, the methods utilized are introduced, second these methods are tried against three different wind tunnel experiments, namely the HART II, 7AD and ERATO blade, and third a parametric study, in which the geometry of the 7AD blade is altered, is performed before concluding the paper.

METHODOLOGY

The general simulation process is outlined in Fig. 1. With the comprehensive code HOST developed by Airbus Helicopters (Ref. 13), an initial trim is initiated using the BET. From this initial trim, the deformations are passed onto the flow solvers, which are either the Unsteady Panel Method (UPM) (Ref. 14) or the CFD code FLOWer (Ref. 15). After they produced periodically converged solutions, the airloads are passed back to the comprehensive code HOST, which again, re-trims the rotor with the new loads and iterates this process until an equilibrium of forces is reached. The coupling is done according to the delta airloads approach (Ref. 16) and has been validated by Yin et al. (Ref. 17) for the UPM-HOST coupling and by

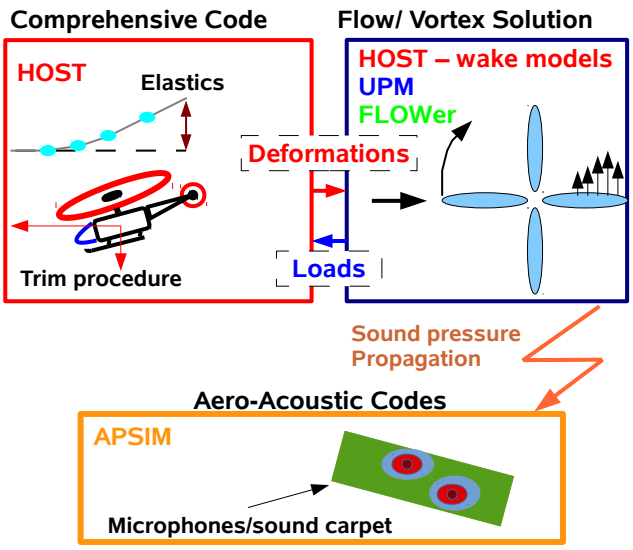

Fig. 1: Process chart of the aero-acoustic simulation

Dietz et al. (Ref. 18) for the FLOWer-HOST coupling. After convergence the aero-acoustic code APSIM (Ref. 19) is called to evaluate the sound pressure at the microphone locations below the rotor.

Acoustic Computation

The here utilized acoustic code is APSIM (Ref. 19), which is based on the Farassat 1A formulation of the Ffowcs-Williams Hawkins (FW-H) equations (Ref. 20). As input data, it either utilizes the lift distribution on the rotor blades as produced by comprehensive codes or the pressure distribution on an acoustic surface. While APSIM can handle porous or permeable surfaces, they have not been employed in this research, since no shocks are expected and therefore the blade surface pressure should suffice for modelling BVI noise. Since an aeroelastically coupled simulation is sought, the effect of elastic deformation is also taken into account according to the methodology by Hennes and Brenntner (Ref. 21). The blade motion as well as the pressure derivatives are obtained through second order finite differencing.

Airloads Simulation

Since the FW-H equations are utilized to transport the acoustic signal over a larger distance, the overall computational burden has already been greatly reduced in contrast to pure computational aero-acoustic (CAA) tools. However, the frequency content of the BVI phenomenon needs still to be resolved by the given flow solution. In Fig. 2 the general dilemma with the aerodynamic simulation of helicopter rotor blades is depicted. While simplified methods such as the BET with a wake model have good turnaround times, their fidelity is rather low in contrast to then over-proportionally expensive simulation codes such as CFD. Their respective theories and merits, along with their shortcomings is reviewed in the next paragraphs.

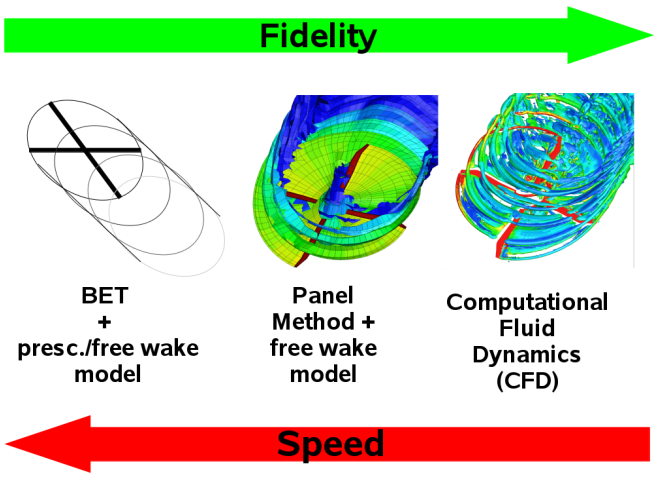

Fig. 2: Trend of fidelity and computational speed of the set of given methods.

Table 1: Individual discretization for each method including timestep in degrees and grid size for CFD

location	radial	chord	time step [°]
P.WAKE	39	1	2
F.WAKE	39	1	2
Oneshot UPM	17	49	2
Coupled UPM	17	49	2
Euler	80 → 40 Mio grid cells	144	0.1
RANS	80 → 40 Mio grid cells	144	0.1

BET with wake models The Helicopter-Overall-Simulation-Tool (HOST) ships with two wake modelling methods: a prescribed wake module called METAR (Ref. 6) and a free-wake module called MESIR (Ref. 5). The regular BET does not take into account the effect of the tip-vortex interaction with the blades, despite the fact that the Prandtl tip loss factor or similar may be utilized. To overcome this, wake modelling has been introduced, which simulates the rotor wake and tip vortices by a vortex-lattice method. A prescribed wake method, such as METAR evolves the wake geometry according to semi-empirical path which takes into account the number of blades, flight path, and overall thrust. Opposing this, the free-wake modelling approach evolves the wake according to the induced velocities which the wakes generates onto itself. While the latter includes more physics, the former is faster and more robust in its convergence. A general difficulty with the wake models is that their theory is based on potential flow. Thus, viscosity is not included in the model itself, but may be partially included through the use of core radius models for the vortices. However, they are often also based on empirical findings as is the case for the HOST models. Even though the wake is now included in contrast to the regular BET, the forces and moments acting on the blade are computed on the quarter chord line of the rotor using 2D sectional airfoil polars, which cannot take into account real 3D effects.

Results with METAR or MESIR are simply labeled **P.WAKE** or **F.WAKE**. The simulations are carried out as isolated rotor simulations using 39 radial sections and 180 azimuthal steps, see Table 1 for comparison with the other methods.

Unsteady Panel Method The Unsteady Panel Method (UPM) (Ref. 22) alleviates the effect of missing out on the 3D modelling. The blade surface is panelized and thus includes the displacement effect of the rotor. Also, the pressure distribution on the surface and the fuselage is now obtained, which allows for a more granular resolution of the BVI phenomenon. The panel method is then coupled with a free-wake model, which has the same up- and downsides as the free-wake model MESIR in HOST. However, good results have already been achieved by Yin et al. (Ref. 14) for the HART II test case. Additional short comings of UPM: it is inviscid and incompressible. While the latter is corrected with the Prandtl-Glauert correction, viscosity is not part of the UPM simulation (yet).

Two employment modes of UPM are tested here. The first is a one-way coupling with HOST-METAR. The trim solution is computed with HOST-METAR to account for viscosity and compressibility from the 2D airfoil polars for the trim solution. With the given trim solution, the pitch control angles as well as the elastic deformations are passed onto UPM, which then runs for four revolutions before the blade surface pressure of the last revolution is passed onto APSIM. The second variant is a delta airloads coupling with the plain BET of HOST, yet only lift is coupled. The reason behind this is that the pitching moment as well as the drag are not correctly predicted with an inviscid method, yet the error made in the lift prediction is negligible. This approach is more costly due to the iterative coupling procedure, but should yield better trim control angles. In both simulations, the fuselage is included as a panelized surface to take into account the displacement effect. Lim et al. (Ref. 23) observed in their CFD simulations that including the fuselage greatly increased the correlation with the experimental data. The time step used here is equivalent to 2^o rotor azimuth, while the surface is resolved with 49 chordwise and 17 spanwise panels (Table 1). The wake is truncated after two revolutions for the sake of fast turn-around times. The two modes are referred to as **Oneshot UPM** and **Coupled UPM**, respectively.

Computational Fluid Dynamics The here utilized flow solver is DLR's FLOWer (Ref. 15). It is a block-structured CFD code, which allows for the solution of the Euler and RANS equations. For acceleration, multigrid, dual-time stepping and residual smoothing are available. Beside the second order Jameson-Schmidt-Turkel scheme (Ref. 24), an implicit forth order compact Pade scheme according to Lele (Ref. 25) has been implemented by Enk (Ref. 26) into the code. Wilke (Ref. 10) was able to obtain good results for the HART II

Table 2: Descent flight conditions and sense of rotation of the different rotors: cw=clockwise, ccw=counter clockwise

	HART II	7AD	ERATO
$N_b[-]$	4	4	4
$R[m]/[ft]$	2.0 / 6.56	2.1 / 6.89	2.1 / 6.89
$RPM[1/min]$	1042	1022	946
$\alpha_c[^\circ]$	4.50	4.33	4.30
$C_t/\sigma[-]$	0.594	0.533	0.631
$\mu[-]$	0.150	0.154	0.165
$M_{tip}[-]$	0.638	0.660	0.616
$M_\infty[-]$	0.096	0.102	0.102
Sense of rotation	ccw	cw	cw

test case using a mixture of the second order and forth order schemes. The same mechanism is applied here. Using the Overset/Chimera technique (Ref. 27), the fuselage as well as the rotor blades are computed using the second order scheme for robustness. The background meshes, in which the blade tip vortices as well as the wake are convected, are then computed using the fourth order Pade scheme.

The major downside of CFD is that the computational cost is tremendous especially in lieu of the other methods. The second downside is the inherently given numerical viscosity required to stabilize the simulation. However, this effect can be traded in for runtime. Increasing the number of grids points and the order of the numerical scheme will decrease the effect of the numerical viscosity at the cost of longer simulations and often less stability.

Again, two simulations variants are setup: On the one hand, inviscid Euler simulations are performed excluding the fuselage, and on the other hand viscous RANS simulations using the Menter SST model (Ref. 28) including the fuselage are performed. The here chosen time step is equivalent to 0.1^o rotor azimuth. Both simulations are coupled, however the Euler simulation is only lift coupled for the same reason as UPM. For comparison of the resolution with the other methods, consult Table 1. The mesh setups consist of 40 million mesh points with a grid spacing of $0.11c$ in vicinity of the rotor. The labels for these simulations are **Euler** and **RANS**. The meshes themselves have been generated with the in-house grid generator G^3, which is based on transfinite interpolation (Ref. 29).

COMPARISON OF VARIOUS METHODS FOR SELECTED ROTOR BLADES

The just mentioned methods are used to investigate the following rotor blades in descent flight: HART II (Ref. 2), 7AD and ERATO (Ref. 30). Each blade is investigated in previous wind tunnel experiments and they represent various generations by aero-acoustic means with the ERATO blade being the most advanced design. The descent flight conditions of the rotor blades are listed in Table 2.

HART II

In Fig. 3, the trim results and the mean airloads for the experiment and the various simulations are plotted. **P.WAKE**

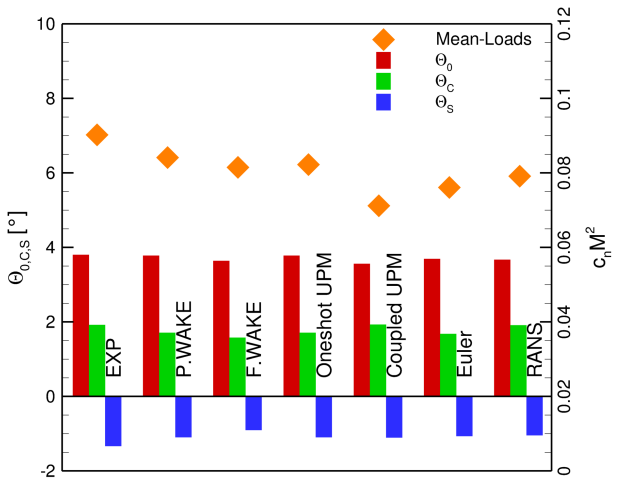

Fig. 3: **HART II** - trim control angles and average airloads ($\overline{c_n}M^2(r/R = 0.87)$)

matches the collective pitch well, yet the cyclic pitches show small deviations to the experiment. Although **F.WAKE** is of higher theoretical fidelity compared to **P.WAKE**, the offsets to the experiment are larger for all pitch angles. **Oneshot UPM** receives its angles from the trim calculation with **P.WAKE** and therefore are the same as pure **P.WAKE**. The collective pitch of **Coupled UPM** has the largest offset to the experiment of all simulations, while the longitudinal cyclic pitch agrees with the experiment. The lateral cyclic pitch has a similar offset as **P.WAKE** has. Both **Euler** and **RANS** calculate collective and lateral cyclic pitch angles close to the experiment. The only difference lies in the longitudinal cyclic pitch, for which the deviation from **Euler** is similar to **P.WAKE** with **RANS** matching the experiment the best.

The average loads are under predicted by all methods with **P.WAKE**, **F.WAKE** and **Oneshot UPM** being the closest to the experiment. **Coupled UPM** shows the largest offset with both CFD (**Euler**, **RANS**) results in between the other methods.

The noise carpet of the HART II experiment is drawn in Fig. 4 at a blade passing frequency (BPF) of $8-20[-]$ being the dominant BVI frequency range. The typical BVI noise peaks are located on the advancing ($\psi \approx 90^o$) and delayed on the retreating side ($\psi \approx 330^o$) of the blade. In addition to the rotor radius the sense of rotation is plotted for easier orientation.

The temporal derivatives of the airloads are graphed in Fig. 5 for the wake simulations (**P.WAKE**, **F.WAKE**) along with their experimental values and respective noise carpets.

The oscillations in the airloads plot and the emitted noise seen on the carpet are directly connected. In Fig. 5a the location of the first peak in the airloads plot of the experiment is found near $\psi = 60^\circ$ on the advancing side of the blade and it has its highest sound pressure level (SPL) around $\psi = 90^\circ$. This delay of 30^o is also observed for both, **P.WAKE** and **F.WAKE**,

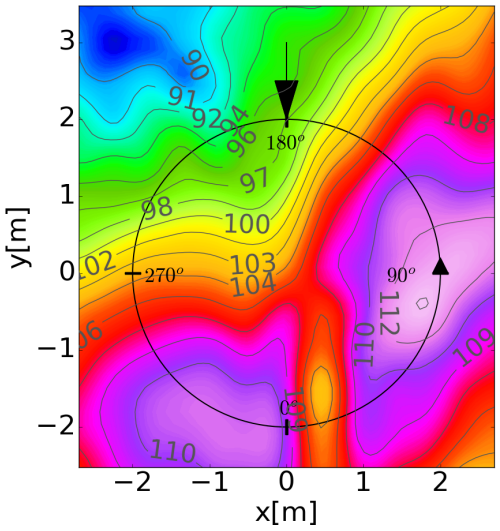

Fig. 4: **HART II** - SPL [dB] - experiment

when looking at Fig. 5b and 5c, respectively. In contrast to the experiment, the wiggles in the airloads are phase shifted, which also results in a shifted peak in the noise carpet. In addition to this, the maximum SPL is under predicted by $3dB$. The second BVI peak is not simulated at all. The wiggles for the **F.WAKE** simulations are more in phase with the experiment (Fig. 5c), but the amplitudes on the advancing and retreating side are larger. Thus the noise level is higher and the peaks are not as isolated as the ones in the experiment. This comes from the generally larger area the wiggles cover for the **F.WAKE** simulation in the airloads plots.

The results of the UPM simulations are displayed in Fig. 6, where the phase of the wiggles and their amplitudes for both methods are better aligned with the experiment than those of **P.WAKE** or **F.WAKE**. Due to the small deviations observed for **Oneshot UPM**, the location of the peak and its noise level shown in Fig. 6b are consistent with the experiment. **Coupled UPM** produces smaller peaks in the loading and thus the overall SPL seen in Fig. 6c is lower than the experiment. Especially on the retreating side of the blade the second peak is not predicted as well as for **Oneshot UPM**. The 30° phase shift as already observed for the experiment and the wake models simulations is also given for UPM both simulations.

Despite the fact that the CFD simulations are considered to be the highest fidelity in comparison with the wake and UPM solutions, their noise prediction is rather disappointing. On the one hand, the oscillations of the airloads in Fig. 7a align better with the experiment than those of the wake models. On the other hand, their amplitudes and thus their SPL on the noise carpet is lower as seen in Fig. 7b and 7c. For the **Euler** method, the location of the peak on the advancing side of the blade is pushed upstream compared to the experiment and is about $2-4dB$ quieter. The noise level of the second peak is also smaller, although it is better captured as for **Coupled UPM**. For the **RANS** simulation, the overall trend is that the

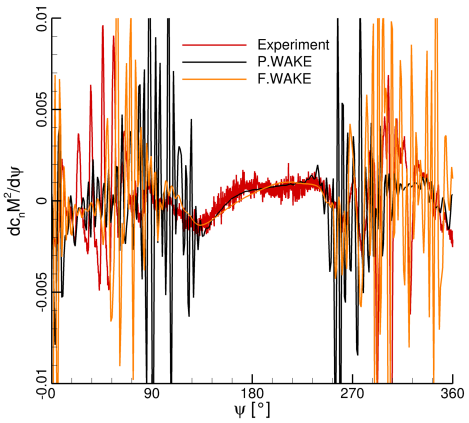

(a) airloads derivatives at $r/R = 0.87$

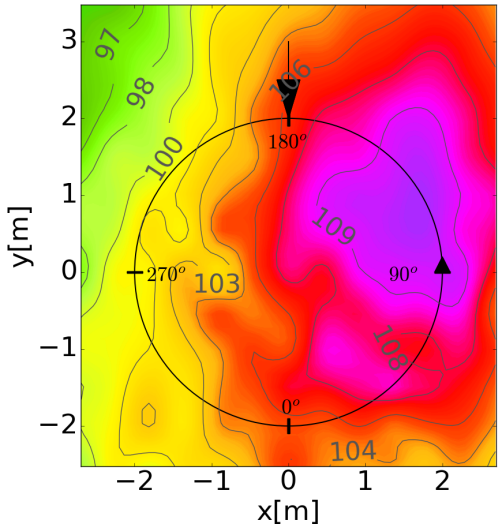

(b) SPL [dB] - **P.WAKE**

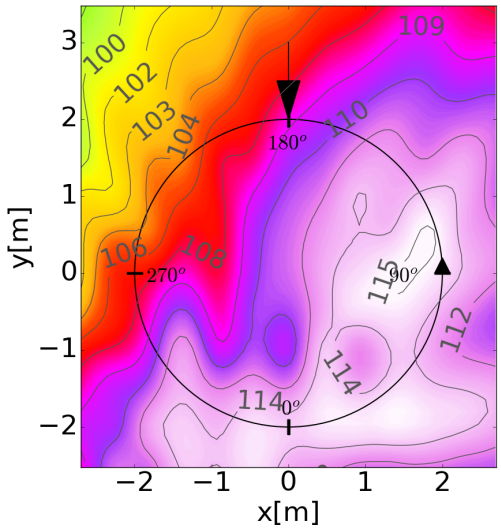

(c) SPL [dB] - **F.WAKE**

Fig. 5: **HART II** - results of **P.WAKE** and **F.WAKE** simulations

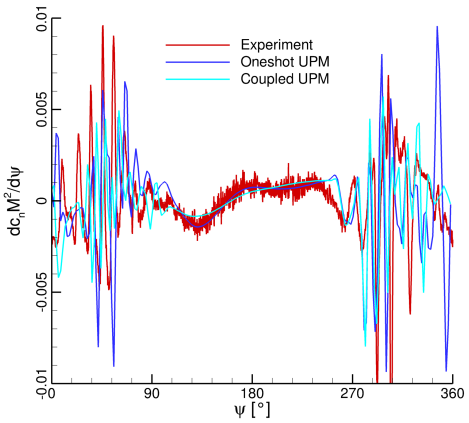

(a) airloads derivatives at $r/R = 0.87$

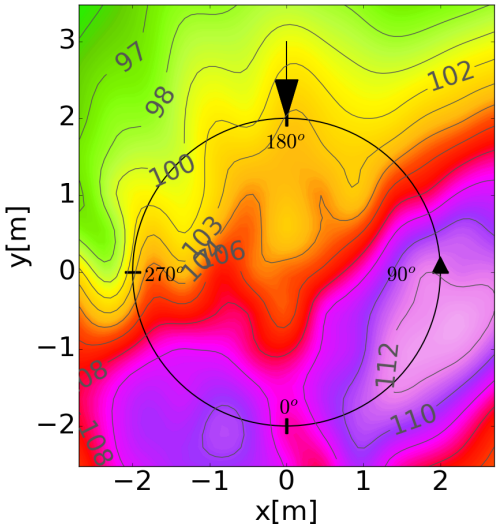

(b) SPL [dB] - **Oneshot UPM**

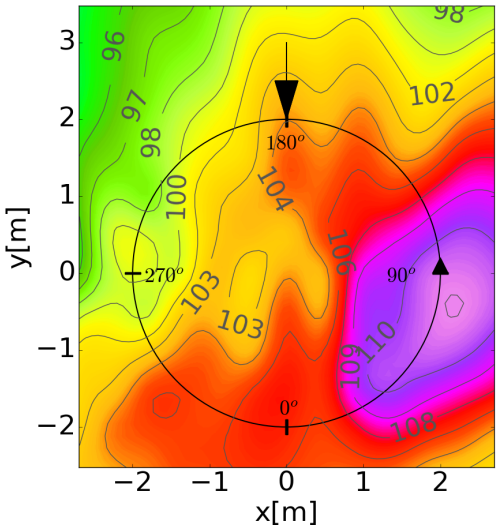

(c) SPL [dB] - **Coupled UPM**

Fig. 6: **HART II** - results of the **UPM** simulations

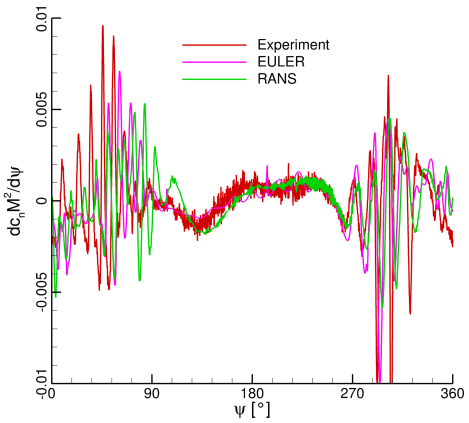

(a) airloads derivatives at $r/R = 0.87$

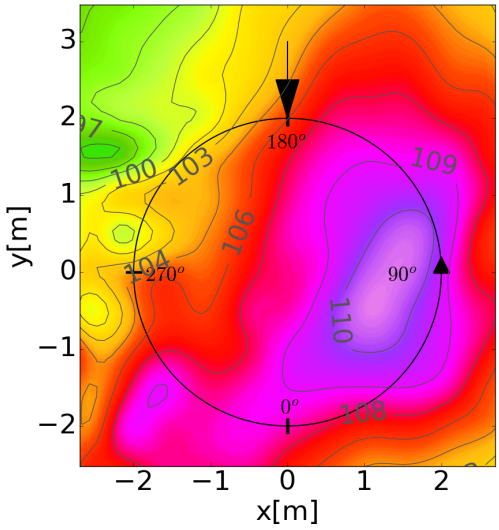

(b) SPL [dB] - **Euler**

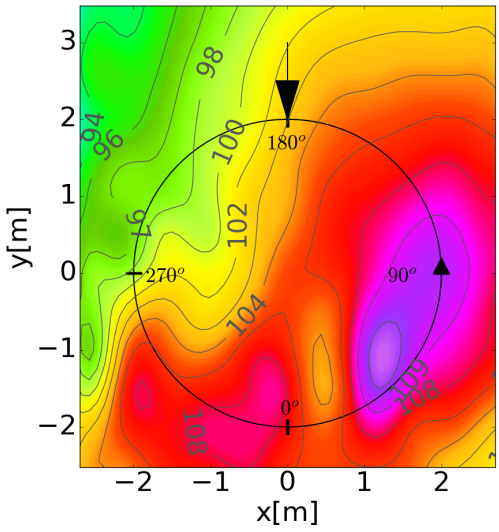

(c) SPL [dB] - **RANS**

Fig. 7: **HART II** - results of the **CFD** simulations

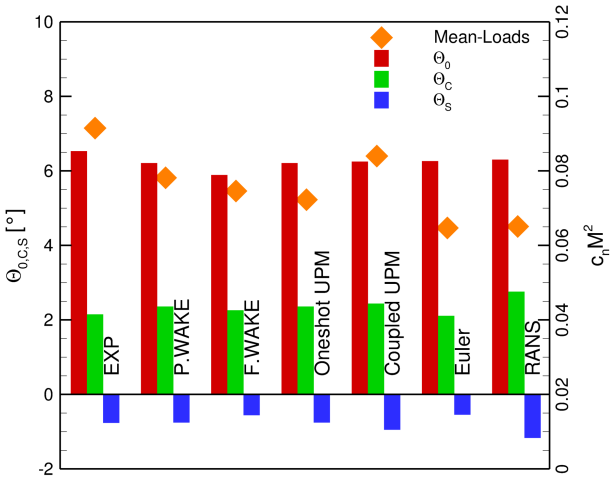

Fig. 8: **7AD** - trim control angles and average airloads ($\bar{c_n}M^2(r/R = 0.825)$)

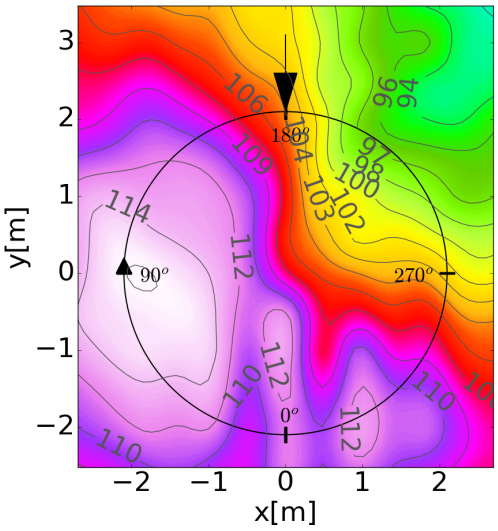

Fig. 9: **7AD** - SPL [dB] - experiment

amplitudes of the airloads oscillations along with the noise levels are reduced. The directivity has improved with respect to the experiment due better trim control angles and the two peaks are more distinct in the simulation, Fig. 7c. The reason why both CFD methods are quieter than the experiment arises from that fact that a relatively small number of grid cells has been used. Wilke (Ref. 10) was able to improve on this fact by using a similar setup that contains more grid cells for the HART II test case.

7AD

The trim angles and the average airloads for the 7AD rotor blade are shown in Fig. 8. For **P.WAKE**, the collective pitch is slightly below the experimental value and the lateral cyclic is above it. The longitudinal cyclic pitch is in good agreement with the experiment. The collective and longitudinal cyclic pitch for the **F.WAKE** simulation have a greater discrepancy to the experiment compared to **P.WAKE** with the lateral cyclic pitch better captured. For **Coupled UPM** the collective and longitudinal cyclic pitch angles are under predicted while the lateral cyclic is over predicted. For the **Euler** calculation the collective and the lateral cyclic pitch are close to the experiment, while the longitudinal cyclic has the largest offset compared to the experiment. The collective pitch of the **RANS** simulation is captured equally well for the **Euler** method. Both cyclic pitch angles have the largest deviation of all simulations with respect to the experiment.

The average airloads are under predicted by both wake simulations, **Coupled UPM** and **Euler**. **Oneshot UPM** over predicts the loads while **RANS** is the closest to the experiment.

The noise carpet of the 7AD experiment is depicted in Fig. 9. Even though the 7AD blade is a more advanced design than the HART II blade, its noise level is higher. This is due to the fact that the 7AD produces more thrust and it is slightly longer than the **HART II** blade. Additionally, the 7AD noise carpet has a second and third peak on the retreating side of the blade.

The results of the wake based simulations for the 7AD are pictured in Fig. 10. The amplitudes of the airloads oscillations of the **P.WAKE** and **F.WAKE** simulations are mostly larger than those of the experiment. In particular the **F.WAKE** simulations has many more wiggles on the retreating side, leading to a similar trend as for the HART II simulations: The directivity on the noise carpet is shifted for both methods, **P.WAKE** and **F.WAKE** and the overall SPL is higher than in the experiment, check Fig. 10b and 10c. The peak on the advancing side is also split into to maxima, which is not observed in the experiment.

The airloads derivatives and the noise carpets of the 7AD simulations with UPM are given in Fig. 11. The oscillations and their amplitudes better align with the experiment (Fig. 11a) compared to the results of the wake models. Larger differences between the simulations and the 7AD experiment are seen for **Oneshot UPM** in Fig. 11b than for **Coupled UPM** in Fig. 11c, for which the noise level in the main peak is under predicted by about $1-3dB$. Unlike for the **HART II** case, **Oneshot UPM** does not capture the second nor the third peak and gives only a crude representation of 7AD noise carpet. **Coupled UPM** simulates a larger main peak on the advancing side and fails to capture the smaller peaks properly. The middle peak near $\psi = 0°$ is similar to the experiment, while its neighbor around $\psi = 315°$ dissolves into a twin peak.

The 7AD results of the CFD computations also show a similar trend as for the HART II case. The phase of the wiggles on both the advancing and retreating side of the blade are in good agreement with the experiment, Fig. 12. Their amplitudes are smaller, hence the amount of noise that is produced is also smaller than for the experiment, shown in Fig. 12b and 12c.

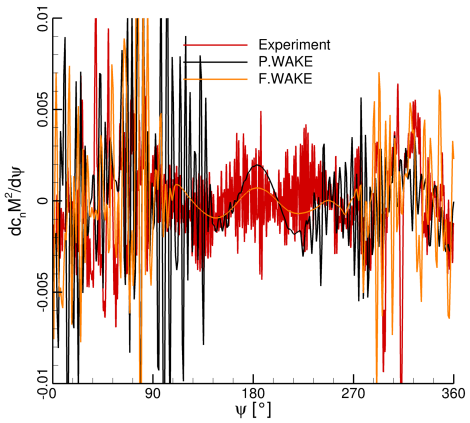

(a) airloads derivatives at $r/R = 0.825$

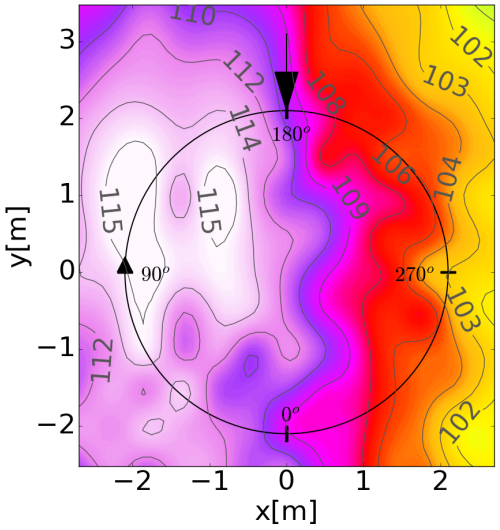

(b) SPL [dB] - **P.WAKE**

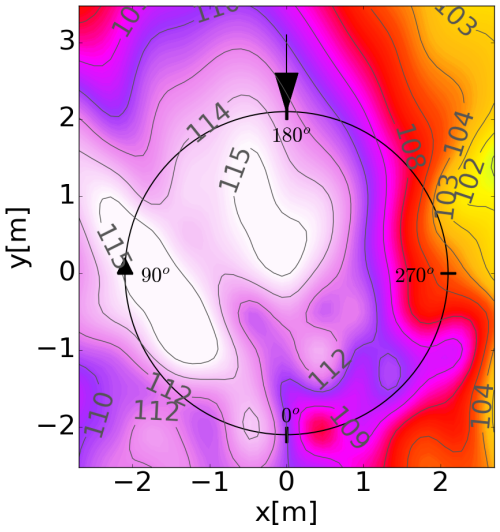

(c) SPL [dB] - **F.WAKE**

Fig. 10: **7AD** - results of **P.WAKE** and **F.WAKE** simulations

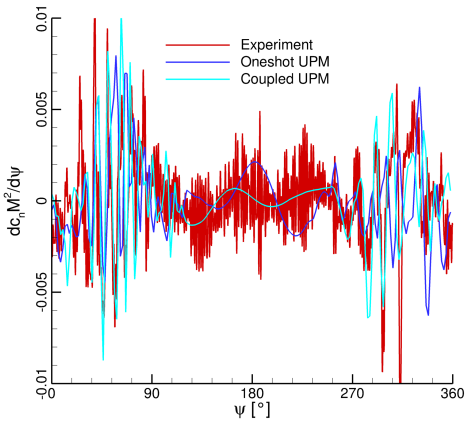

(a) airloads derivatives at $r/R = 0.825$

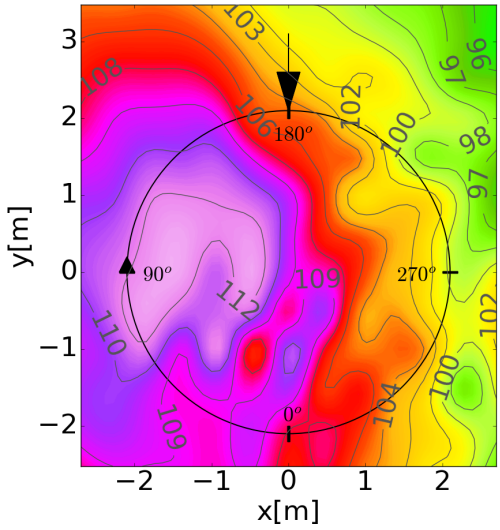

(b) SPL [dB] - **Oneshot UPM**

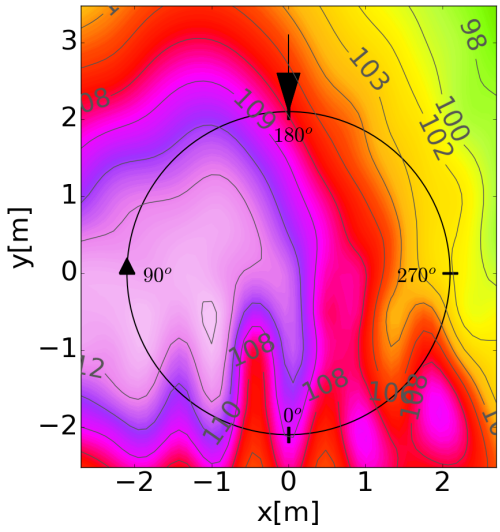

(c) SPL [dB] - **Coupled UPM**

Fig. 11: **7AD** - results of the **UPM** simulations

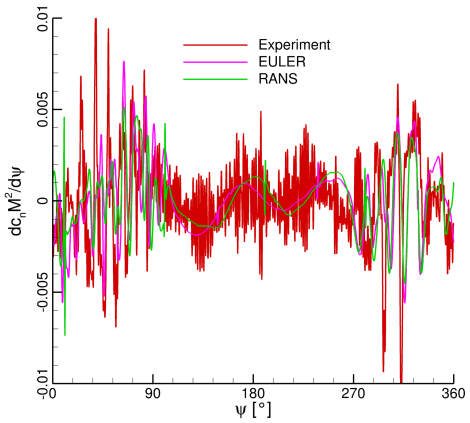

(a) airloads derivatives at $r/R = 0.825$

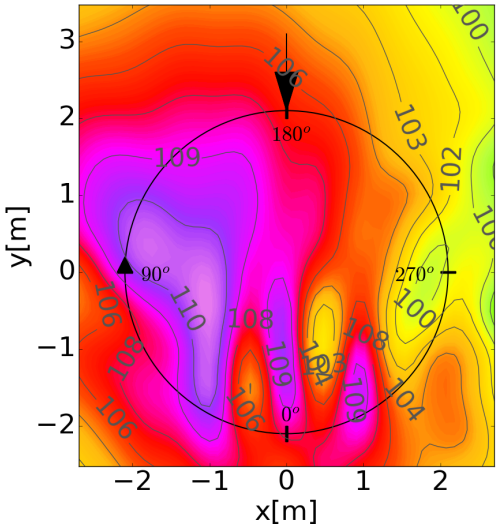

(b) SPL [dB] - **Euler**

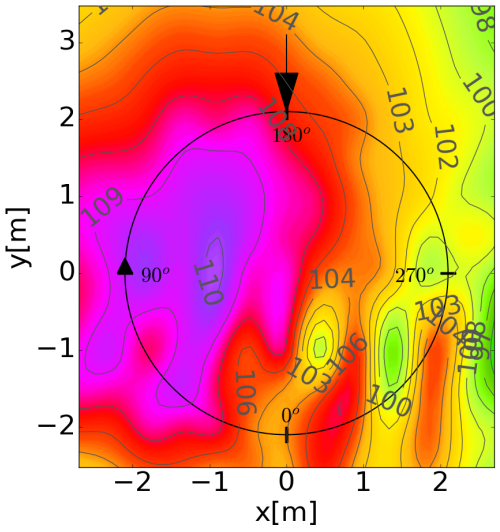

(c) SPL [dB] - **RANS**

Fig. 12: **7AD** - results of the **CFD** simulations

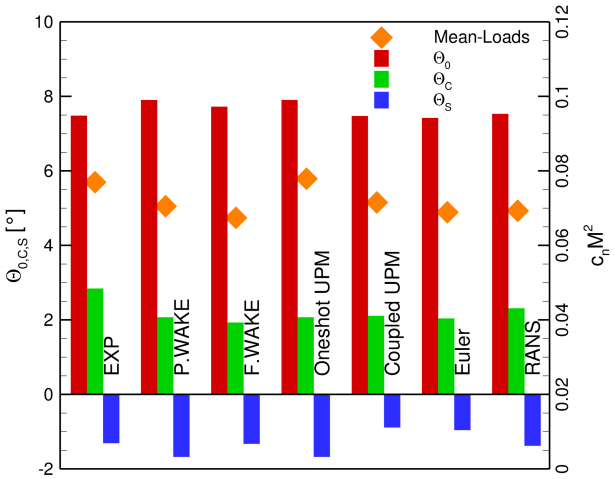

Fig. 13: **ERATO** - trim control angles and average airloads ($\overline{c_n}M^2(r/R = 0.85)$)

The SPL of the main peak is about $5dB$ too low, however the second and third peaks on the retreating side are captured by both methods in contrast to the previously investigated methods.

ERATO

The trim angles plotted in Fig. 13 for **ERATO** simulations show that **P.WAKE** over predicts the collective pitch angle and under predicts both the lateral and longitudinal cyclic angles. The collective and the longitudinal cyclic pitch angle predicted by **F.WAKE** correlate well with the experiment, yet the lateral cyclic has an even larger offset with the experiment than **P.WAKE**. **Coupled UPM** finds a collective pitch angle close to the experiment, but the lateral cyclic has a similar level as **P.WAKE** and the longitudinal cyclic has the largest offset among all methods. The trim angles of the **Euler** simulation are similar to the **Coupled UPM** results with slight deviations in cyclic angles. Except for the lateral cyclic pitch, the **RANS** simulation computes the trim angles close to their experimental values. Both wake methods, **Coupled UPM** and both CFD simulations under predict the average airloads minor deviations. Only the **Oneshot UPM** predicts the average load close to the experiment.

The ERATO blade is a blade specifically designed with a forward-backward sweep to reduce the amount of emitted noise. Together with a reduced RPM, the ERATO blade is about $6dB$ quieter than the 7AD blade, refer to Fig. 14. The experimental noise carpet features one major peak on the advancing side, while the two intermediate peaks also present for the 7AD blade are strongly reduced.

The wake based methods **P.WAKE** and **F.WAKE** over amplify the wiggles in the airloads derivatives Fig. 15a. Contrary to what has been observed so far, the peak in the noise carpet plot Fig. 15b is quieter by about $3db$ to the experimental

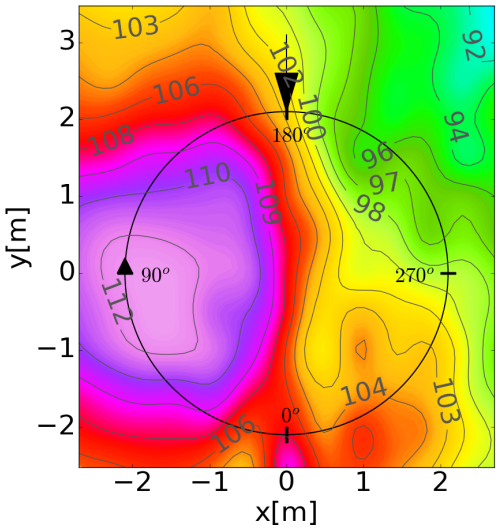

Fig. 14: **ERATO** - SPL [dB] - experiment

value. Due to the erroneously captured wiggles of **F.WAKE** at $\psi \approx 10^o$ found in the airloads plot, the noise carpet shows an additional strong peak. Since the amplitude of these wiggles is greater than those of the experiment, the peak values on the noise carpet are also louder by $2dB$.

The airloads for the UPM simulations, depicted in Fig. 16a show a fair agreement with the experiment. The resulting noise carpet for **Oneshot UPM** Fig. 16b features a good directivity in comparison with the experiment, though the peak is louder by $3dB$. **Coupled UPM** also over predicts the noise level by up to $2dB$ and captures parts of the second peak near $\psi = 0°$, Fig. 16c.

Both CFD simulations of the ERATO blade resolve the airloads in phase with the experiment, but their amplitudes are smaller, especially for **Euler**, Fig. 17a. In combination with the smaller amplitudes, it is also observed that the noise is quieter by about $4dB$ for both methods on the advancing side peak, see Fig. 17b and 17b. No second peak on the retreating side is predicted, the directivity of the **Euler** simulation is more round and therefore better aligned with the experiment than the oval shaped advancing side peak for **RANS**.

Review of the Accuracy and Costs

To perform a parametric and optimization study with variable fidelity methods it is important to take the computational costs into account. In Fig. 18 the average computational time required for the various methods is presented. The **RANS** simulations are considered as the highest-fidelty level and thus the reference based on earlier CFD simulations (Ref. 10). The **Euler** simulations take longer, because more iterations to trim the rotor are needed compared to the **RANS** method. The hope was that neglecting the physical friction helps better in conserving vorticity, however no greater gain is observed. More than three orders of magnitude in computational effort lie between the wake models and the CFD calculations.

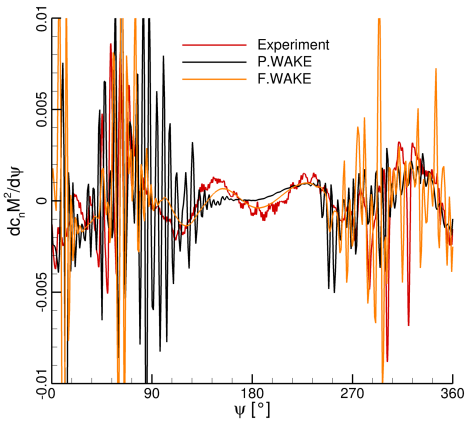

(a) airloads derivatives at $r/R = 0.85$

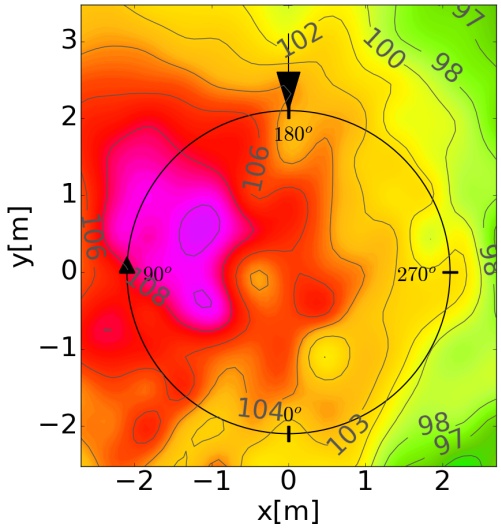

(b) SPL [dB] - **P.WAKE**

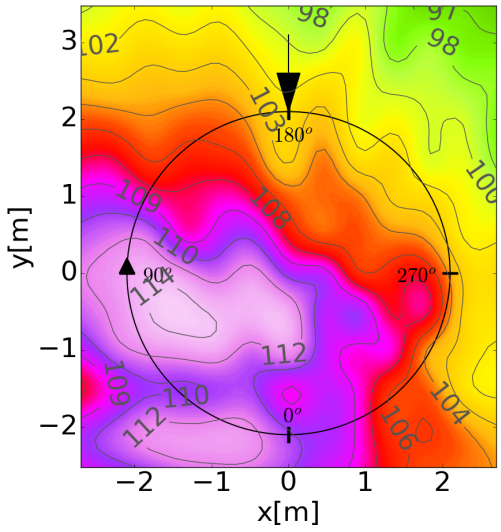

(c) SPL [dB] - **F.WAKE**

Fig. 15: **ERATO** - results of **P.WAKE** and **F.WAKE** simulations

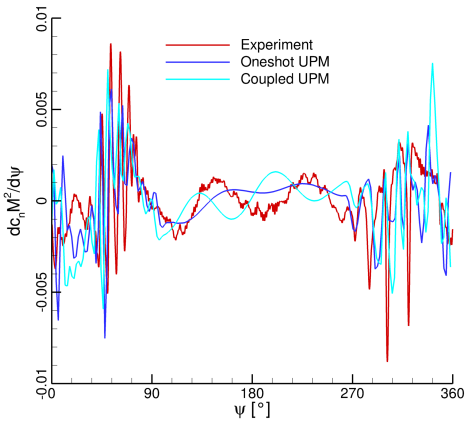

(a) airloads derivatives at $r/R = 0.85$

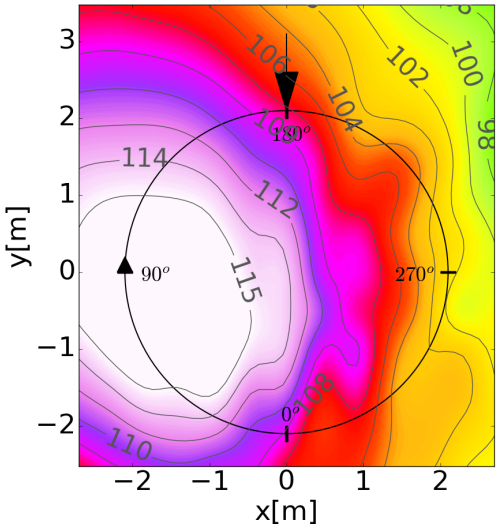

(b) SPL [dB] - **Oneshot UPM**

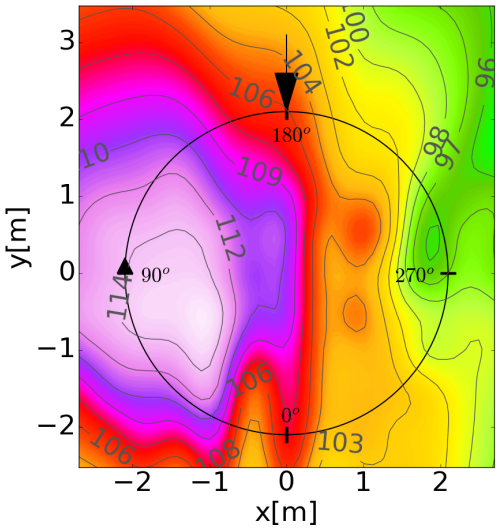

(c) SPL [dB] - **Coupled UPM**

Fig. 16: **ERATO** - results of the **UPM** simulations

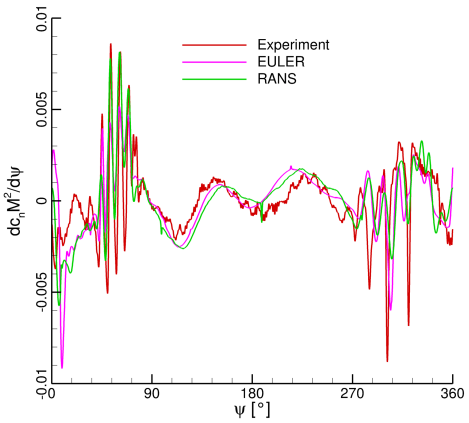

(a) airloads derivatives at $r/R = 0.85$

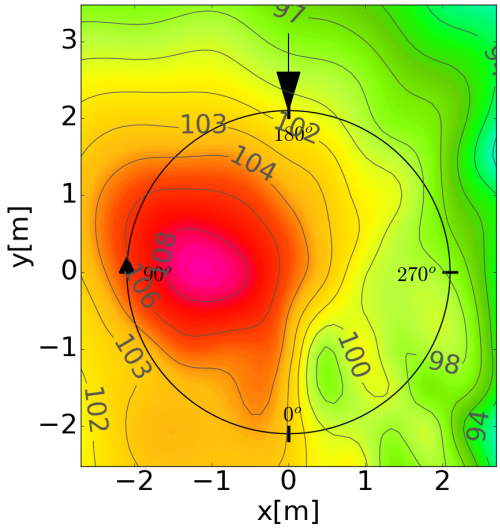

(b) SPL [dB] - **Euler**

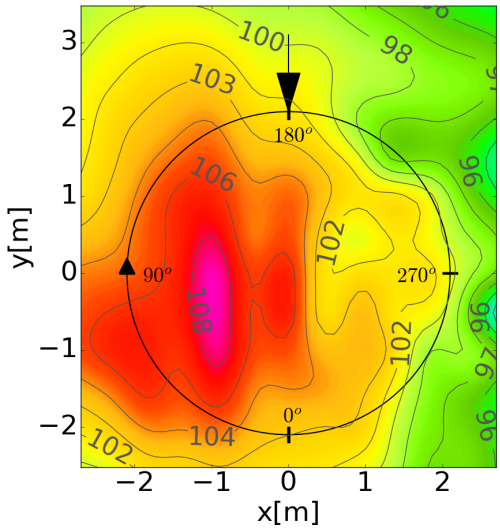

(c) SPL [dB] - **RANS**

Fig. 17: **ERATO** - results of the **CFD** simulations

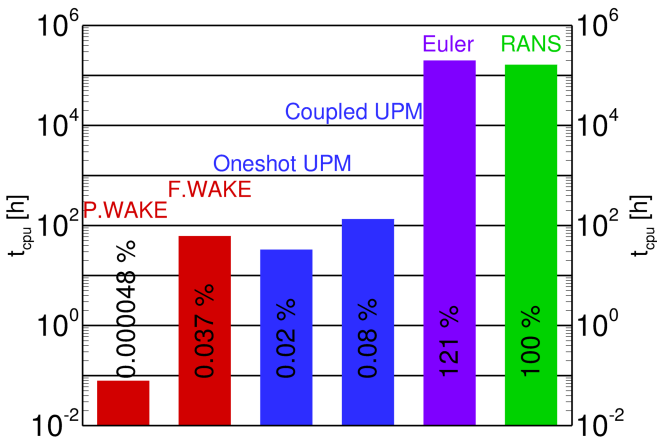

Fig. 18: Average logarithmic scaled time needed for different methods in computational hours

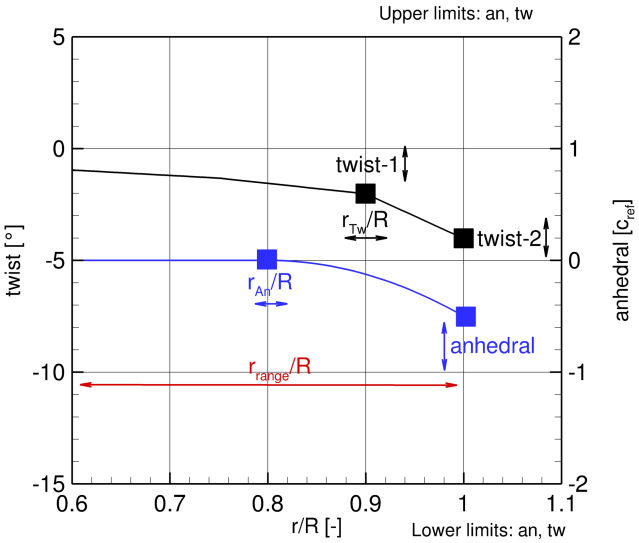

Fig. 19: Rotor blade definiton of the **7AD** baseline

The **F.WAKE** model nearly requires twice as much time as **Oneshot UPM** to finish a simulation with the **Oneshot UPM** results being better. Looking towards designing a rotor, it has to be noted that the trend of maximum noise has been captured by all methods. All of them predicted that the HART II blade is the quietest blade, followed by the ERATO and 7AD blade. Following up on this, the parametric study is continued with **P.WAKE**, which features the fastest method, which also led to more stable results than **F.WAKE** and **Coupled UPM**, which was able to get closest to the experimental values on average. No CFD simulations are carried out due to their tremendous cost.

RESULTS OF THE PARAMETRIC STUDY

For the parametric study the 7AD blade is investigated at the operational flight conditions of the ERATO blade. The difference between the operational 7AD flight condition and the ERATO flight condition is basically a reduction in RPM. During the wind tunnel campaign (Ref. 30), a reduction of $2dB$ in peak SPL has been observed. The question is, which alternative parameters to the double-sweep might aide in the reduction of rotor noise? The first parameter to be looked at is an-/dihedral defined by a vertical blade tip offset and a radial starting location. The blending is done through a cubic spline representation. These parameters are expected to have a strong influence on the rotor noise, as they govern the location of the tip vortex release. The second parameter looked into is the twist distribution, which has a strong effect on performance, but likely not so much on the acoustics. A piecewise linear distribution is chosen, with an inner and outer parameter for the magnitude of the twisting, while additionally the radial location of the inner parameter is altered. The second parameter is located at the tip. Both parameter sets are sketched in Fig. 19 along with their parameter limits without actually representing the 7AD blade. The metric looked into is the maximum SPL value on the noise carpet, which is then mapped into a landscape diagram using Kriging surrogate models.

7AD Baseline Case

Before going into the details about the parameter changes, the baseline case is introduced first. As previously mentioned, the rotor RPM is reduced for the 7AD rotor to the same RPM as for the ERATO blade. In Fig. 21 the disc plot of the airloads derivatives ($dc_n M^2/d\psi$) for the **P.WAKE** simulation is depicted along with the noise carpet. Opposing this, the **Coupled UPM** results are presented in Fig. 22. From these plots it is observed that both methods predict a noise reduction with respect to the original operational conditions of the 7AD blade, compare Fig. 10b and Fig. 11c. However, the trends differ strongly between the methods when it comes to the airloads representation shown in Fig. 21a and Fig. 22a. The maximum SPL of the **P.WAKE** result is $110dB$ and $113dB$ for the **Coupled UPM** solution.

Anhedral

The results of the parametric study of anhedral with **P.WAKE** are displayed in Fig. 23 and 24. The landscape plot and the blade planform of the best **P.WAKE** design of the parametric study are presented in Fig. 23a and 23b. The magenta dots represent an investigated blade planform (sample) and the big magenta diamond marks the best planform for the lowest maximum SPL. Blue areas denote a reduction in emitted noise and red areas denote increased in emitted noise. The simulations with **P.WAKE** were all successful and an upwards directed tip, beginning at a radius of $r/R = 0.6$ is predicted as a beneficial planform to reduce the noise. The maximum ocurring SPL has been reduced to $108dB$, depicted in Fig. 24a. The characteristical noise peaks, as visible for the baseline case, are gone. In the top right corner a large reduction of up to

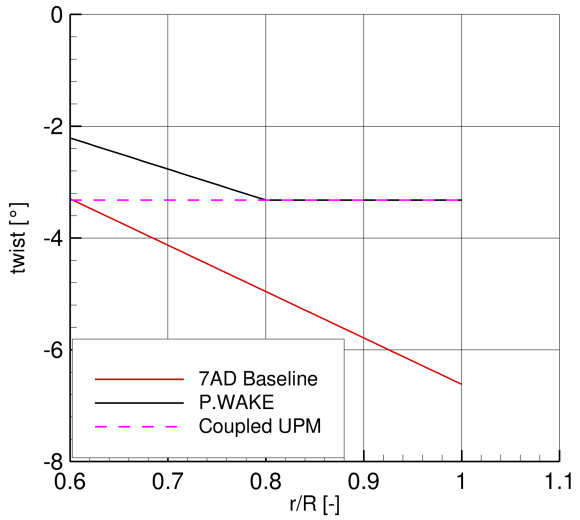

Fig. 20: Results of the twist study

$10dB$ is observed as well as on the advancing side of the blade. In the lower right corner around $\psi = 300°$ the noise has been increased by up to $7dB$ which is depicted in Fig. 24b. Due to the effect of the upwards directed tip, the vortices are set up above the rotor blade so that the following blades do not hit the vortex completely. This effect is seen in Fig. 23c for the airloads derivative, which also explains the reduction in noise. The loads are more focused at the tip in the rear of the rotor. This also explains why the aft section becomes louder in contrast to the baseline.

The simulations with **Coupled UPM** take longer than with **P.WAKE**, therefore less blade designs are investigated in this study. The results are presented in Fig. 25 and 26. In Fig. 25a two spots of low noise are identified in the landscapes, while the black area marks unfeasible designs; no trim solution exists. Just as for the best **P.WAKE** blade an upwards directed tip is predicted as a beneficial design concerning the emitted noise, yet the amount of anhedral is lower and the relative gain in maximum SPL is better. The common BVI hotspots of descent flight are found in Fig. 26a where the noise level reaches $106dB$. The noise reduction observed in Fig. 26b ranges from $3-7dB$. Only a small area in the lower right corner is slightly louder. Similar to the best **P.WAKE** design, the same effect of the new design is observed in Fig. 25c. The peaks in airloads derivatives are more focused at the tip. While both methods are able to predict similar blade designs, the **Coupled UPM** results appear more plausible, however at a greatly increased computational cost.

Twist

The results for the **P.WAKE** twist study are depicted in Fig. 27 and 28 for **P.WAKE**, with the best twist distribution plotted in Fig. 20 along with the baseline and the best **Coupled UPM** blade. Since three parameters are varied, the here shown landscape focuses on the radial cut where the best design is found. From this plot it is observed that only a small band is given for which the twist parameter brings improvement to the 7AD blade. Any change in sign of the twist leads to an increase in noise, which is also observed for the performance. For the best design, the peak noise is reduced to $106dB$ with an overall noise reduction is of about $1-3dB$, compare see Fig. 28a and 28b. The peaks in airloads found in Fig. 27b are not focused on either side of the blade but distributed along the blade span on both the advancing and retreating side. Due to the larger spread of the airload peaks, the noise reduction on the overall noise carpet is less with respect to the best anhedral. The advancing side BVI hotspot is being smeared out over a larger area.

Coupled UPM predicts a similar trend for the twist parameters as **P.WAKE** illustrated by Fig. 29a. The difference to **P.WAKE** is that the severity of the twist alternation is reduced in relative magnitude. The best planform retrieved with **Coupled UPM** predicts a constant twist distribution along the blade beginning at $r/R = 0.6$, depicted in Fig. 20.

The noise peak on the advancing side of the blade in Fig. 30a is not as focused any more but spread from $\psi = 0-100°$. The noise in the rotor area is reduced by $1-5dB$, yet an increase in the lower right corner of Fig. 30b of about $1-5dB$. The vortex trajectories are not directly affected as already mentioned for the **P.WAKE** results, therefore oscillations are not focused at the tip of the blade, refer to Fig. 29b. The reason for the noise increase on the retreating side is explained with the larger amplitudes around $\psi = 300°$.

Again, both methods predict similar trends with **Coupled UPM** offering more plausible results. As for the twist as a parameter itself, it only alters the effect of how the vortices are perceived by the blade, less the vortex trajectories.

CONCLUSIONS

In this paper, different aerodynamic methods for computing helicopter BVI noise have been investigated. The task was split into two sections: First, three different wind tunnel models were simulated with six different methods, each. Secondly, a parametric study has been conducted in which two of the previously six methods are tried against each other to see how well they can predict geometric changes to the rotor. The following observations were made:

1. For the wake based models; it was difficult to find good initial core radius settings that satisfied all wind tunnel tests.
2. The best results for the wind tunnel tests were found using the free-wake coupled panel methods.
3. While CFD should be able to compute better results on finer meshes, the here shown results were roughly 4dB quieter in the BVI peaks for all test cases.
4. From the two investigated parameters, dihedral showed the most promising results in terms of noise reduction.

This is contrary of what has been observed in the literature so far, where an anhedral is preferred. Additionally, the question of whether this blade can be handled dynamically is a remaining question to be answered.

5. From the parametric study it is seen that the design trends align for the BET based and panel method. However, noticeable discrepancies in their predictions exist and should be double-checked with CFD.

REFERENCES

[1]W. F. J. Olsman, and B. I. Schuchardt, "Segmentwise Measurement of Helicopter Approach Noise with a Reduced Microphone Setup," *Journal of the American Helicopter Society*, Vol. 60, (4), 2015, pp. 1–18.
doi: doi:10.4050/JAHS.60.042005

[2]Berend G. van der Wall, "A Comprehensive Rotary-Wing Data Base for Code Validation: The HARTII International Workshop," *The Aeronautical Journal 115, Nr. 1164*, 2011, pp. 91–102.

[3]Berend G. van der Wall, Christoph Kessler, Yves Delrieux, Philippe Beaumier, Marc Gervais, Jean-Francois Hirsch, Kurt Pengel and Pascal Crozier, "From ERATO Basic Research to the Blue Edge Rotor Blade," *AHS 72nd Annual Forum, West Palm Beach, Florida*, 2016, pp. 8.

[4]T.S. Beddoes, "A Wake Model for High Resolution Airloads," Second International Conference on Basic Rotorcraft Research, 1985.

[5]Michea, B. and Chauvin, J., *Etude des sillages de rotors d'helicoptere en vol d'avancement et de leur influence sur les performances du rotor (interaction pale-tourbillon)*, Ph.D. thesis, Université Pierre et Marie Curie (Paris), 1992.

[6]G. Arnaud, B. Benoit and F. Toulmay, "Improvements to the Aerodynamic Model of the R85 Helicopter Rotor Code Validation and Applications," 28^{th} *ISl Applied Aerodynamics Symposium*, 1991.

[7]Boyd, D. D. J., "HART-II Acoustic Predictions using a Coupled CFD/CSD Method," AHS International 65th Forum and Technology Display, 2009.

[8]Marilyn J. Smith, Joon W. Lim, Berend G. van der Wall, James D. Baeder, Robert T. Biedron, D. Douglas Boyd, Jr., Buvana Jayaraman, Sung N. Jung, Byung-Young Min, "An Assessment of CFD/CSD State-of-the-Art Using the HART II International Workshop Data," *AHS International 68th Annual Forum & Technology Display, Ft. Worth, TX*, 2012.

[9]R. K. Jain, J. W. Lim, and B. Jayaraman, "Modular Multisolver Approach for Efficient High-Fidelity Simulation of the HART II Rotor," *Journal of American Helicopter Society*, 2015.

[10]G. Wilke, "Efficient Aero-Acoustic Simulation of the HART II Rotor with the Compact Pade Scheme," 42nd European Rotorcraft Forum, 2016.

[11]Ulrich Kowarsch, Constantin Öhrle, Manuel Keßler, "Aeroacoustic Simulation of a Complete H145 Helicopter in Descent Flight," *Journal of the American Helicopter Society, Vol. 61, (4)*, 2016, pp. 1–4.
doi: 10.4050/JAHS.61.042001

[12]J. Yin, B. v. d. W. and Wilke, G., "Rotor noise radiation under influence of blade deformation, compressibility and different fuselage modelling," *Journal of Sound and Vibration*, Vol. 357, 2015, pp. 115–116.

[13]Bernard Benoit, André-Michel Dequin, Konstantin Kampa, Wolfgang von Grünhagen, Pierre-Marie Basset and Bernard Gimonet, "HOST, a Genereal Helicopter Simulation Tool for Germany and France," *American Helicopter Society 56th Annual Forum, Virignia Beach, Virginia*, 2000.

[14]Jianping Yin, "DLR Free Wake Unsteady Panel Method (UPM) User Handbook for Application of the Rotors," *Report of the Institute of Aerodynamics and Flow Technology*, 2011.

[15]J. Raddatz, and J. Fassbender, "Block structured Navier-Stokes solver FLOWer. MEGAFLOW - Numerical Flow Simulation for Aircraft Design," *Notes on Numerical Fluid Mechanics and Multidisciplinary Design*, Vol. 89, 2005, pp. 27–44.

[16]M. Potsdam, H. Y. and Johnson, W., "Rotor Airloads Prediction Using Loose Aerodynamic/Structural Coupling," American Helicopter Society 60th Annual Forum, 2004.

[17]J. Yin, B. G. van der Wall, and G. Wilke, "Rotor Aerodynamic and Noise under Influence of Elastic Blade Motion and Different Fuselage Modeling," 40th European Rotorcraft Forum, 2014.

[18]Markus Dietz, B. K., Walid Khier, "Numerical Simulations of a Full Helicopter Configuration Using Weak Fluid-Structure Coupling," *46th AIAA Aerospace Sciences Meeting and Exhibit, Reno, Nevada*, 2008.

[19]Jianping Yin, Martin Kuntz and Jan Delfs, "Prediction of Acoustic Far Field with DLR's Acoustic Code APSIM, APSIM manual for version 7.0," Technical report, 2008.

[20]Brentner, K. S. and F.Farassat, "Modeling aerodynamically generated sound of helicopter rotors," *Progress in Aerospace Sciences 39*, 2003.

[21]C. C. Hennes and K. S. Brentner, "The Effect of Blade Deformation on Rotorcraft Acoustics," 31st European Rotorcraft Forum, 2005.

[22]J.P. Yin, and S.R. Ahmed, "Treatment of Unsteady Rotor Aerodynamics Using a 3-D Panel Method," Technical report, Deutsche Forschungsantalt für Luft- und Raumfahrt Forschungsbereich Strömungsmechanik, 1994.

[23]J. W. Lim, and A. C. B. Dimanlig, "The Effect of Fuselage and Rotor Hub on Blade-Vortex Interaction Airloads and Rotor Wakes," 36th European Rotorcraft Forum, 2010.

[24]A. Jameson, W. Schmidt, and E. Turkel, “Numerical Solution of the Euler Equations by Finite Volume Methods Using Runge-Kutta Time-Stepping Schemes,” 14th AIAA Fluid and Plasma Dynamics Conference, 1981.

[25]Sanjiva K. Lele, “Compact Finite Difference Schemes with Spectral-like Resolution,” , 1991.

[26]Stephan Enk, *Zellzentriertes Padeverfahren für DNS und LES*, Ph.D. thesis, TU Braunschweig, 2015.

[27]T. Schwarz, *Ein blockstrukturiertes Verfahren zur Simulation der Umströmung komplexer Konfigurationen*, Ph.D. thesis, Institut für Aerodynamik und Strömungstechnik, DLR, Braunschweig, 2005.

[28]Menter, F. R., Kuntz, M., and Langtry, R., “Ten years of industrial experience with the SST turbulence model. Begell,” , 2003.

[29]L. E. Eriksson, “Generation of Boundary-Conforming Grids Around Wing-Body Configurations Using Transfinite Interpolation,” *AIAA Journal*, Vol. 20-10, 1982, pp. 1313–1320.

[30]W. R. Splettstoesser, K.-J. Schulz and H.Bucholz, “ERATO Rotor Validation Test in DNW - Documentation and Representative Results,” Technical report, DLR - Institut für Entwurfsaerodynamik, 1999.

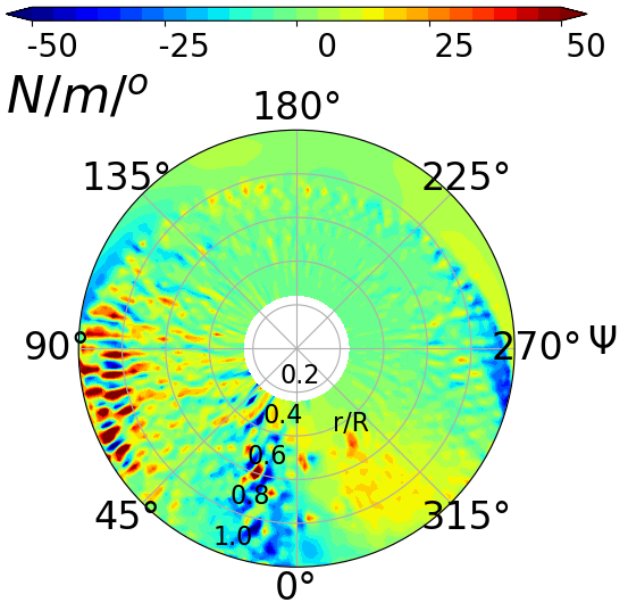

(a) airloads derivatives

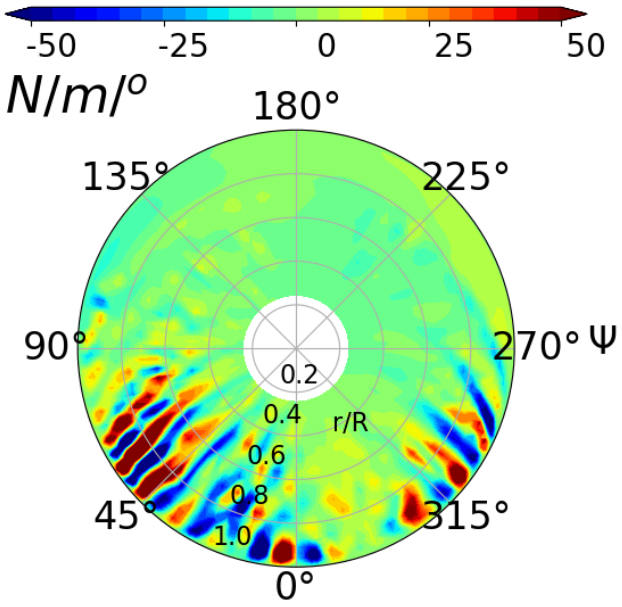

(a) airloads derivatives

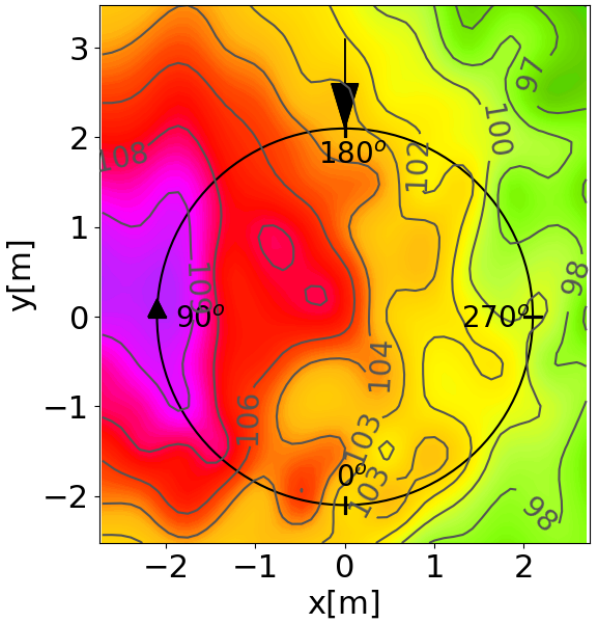

(b) SPL [dB]

Fig. 21: **7AD** baseline case - **P.WAKE** results

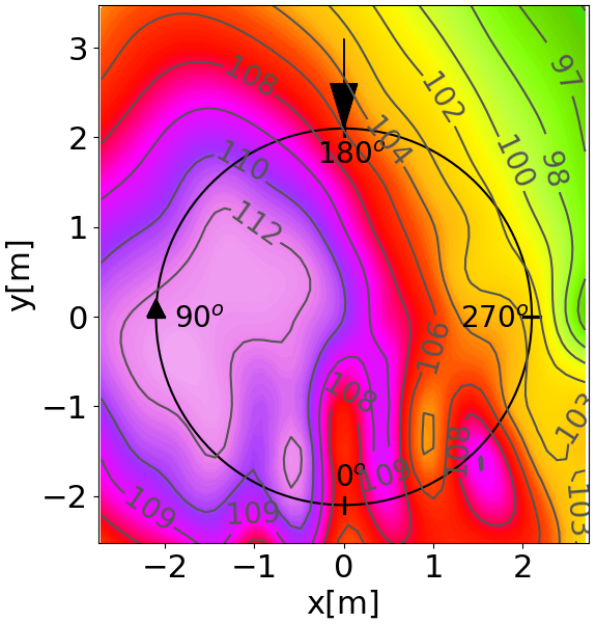

(b) SPL [dB]

Fig. 22: **7AD** baseline case - **Coupled UPM** results

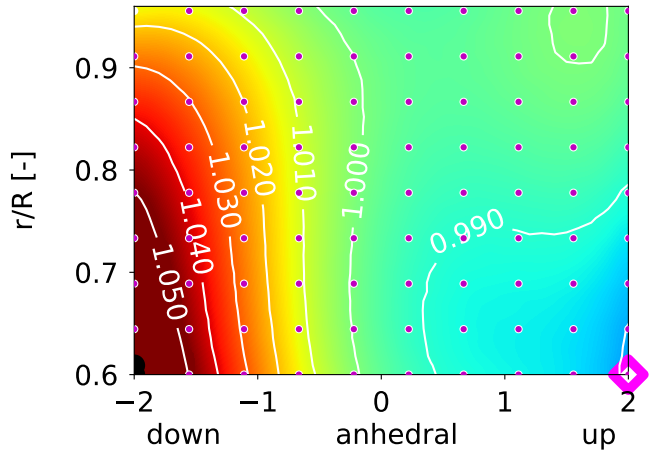

(a) parameter landscape

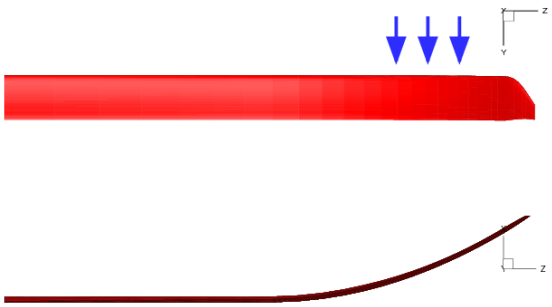

(b) best blade design

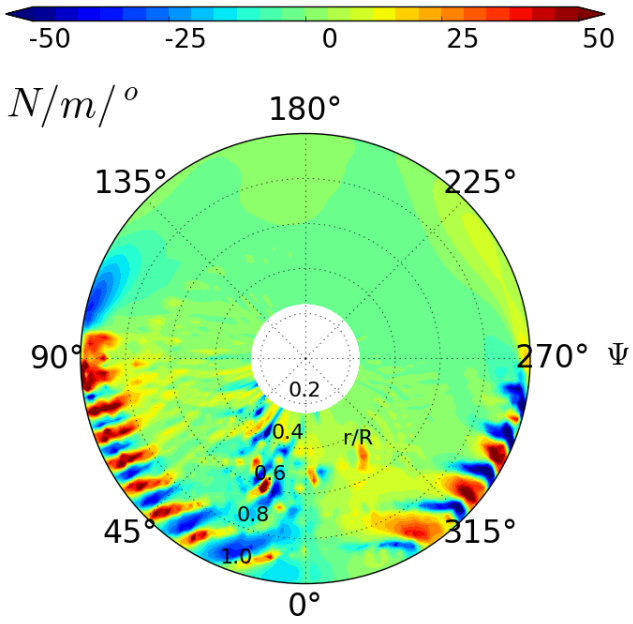

(c) airloads derivatives

Fig. 23: **P.WAKE** anhedral study - results

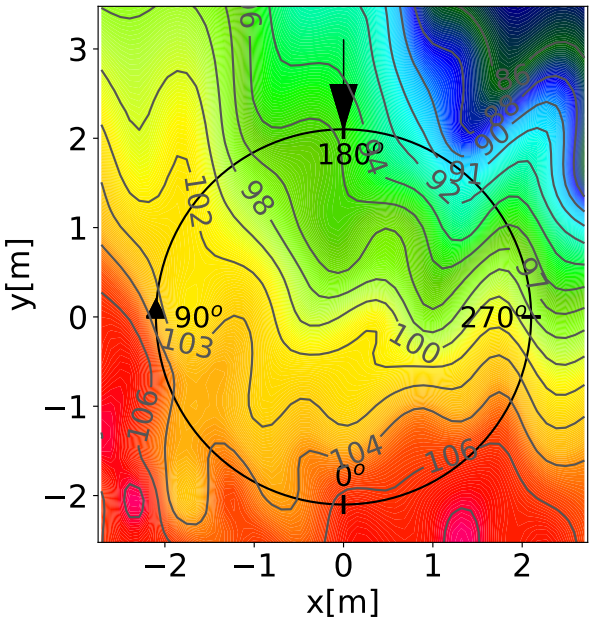

(a) SPL [dB]

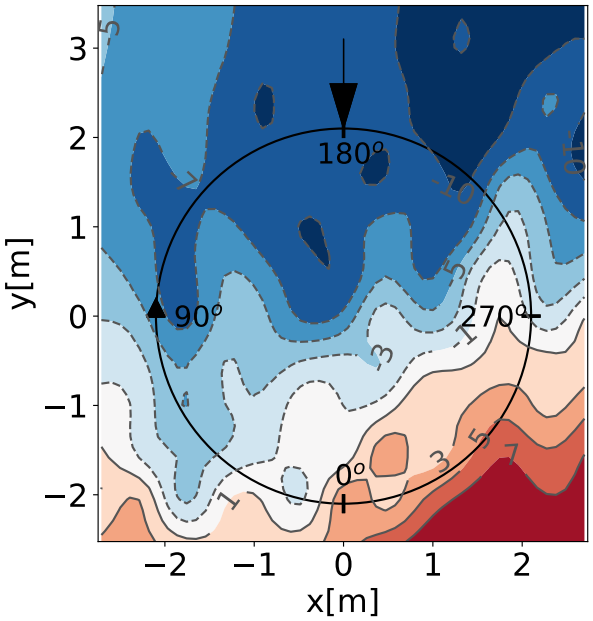

(b) ΔSPL [dB]

Fig. 24: **P.WAKE** anhedral study - noise and delta noise carpets with

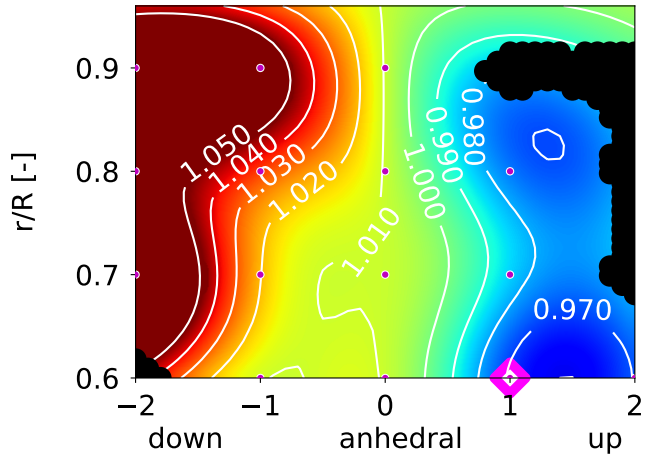

(a) parameter landscape

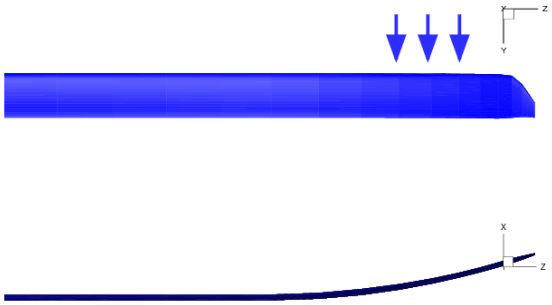

(b) best blade design

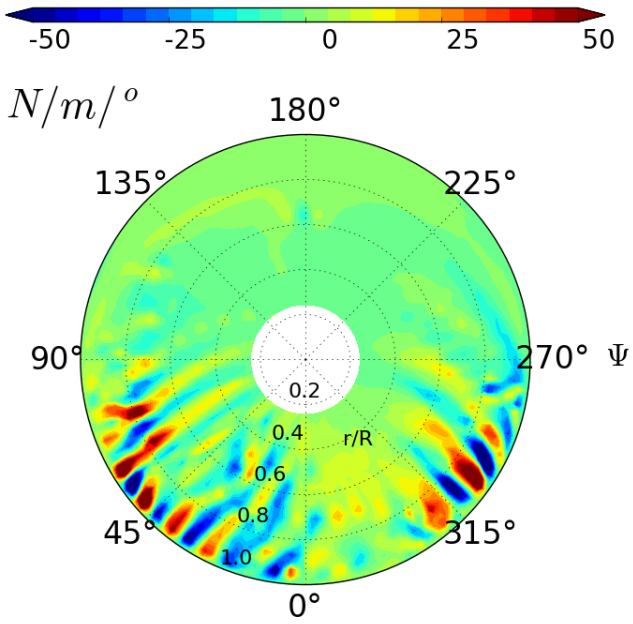

(c) airloads derivatives

Fig. 25: **Coupled UPM** anhedral study - results

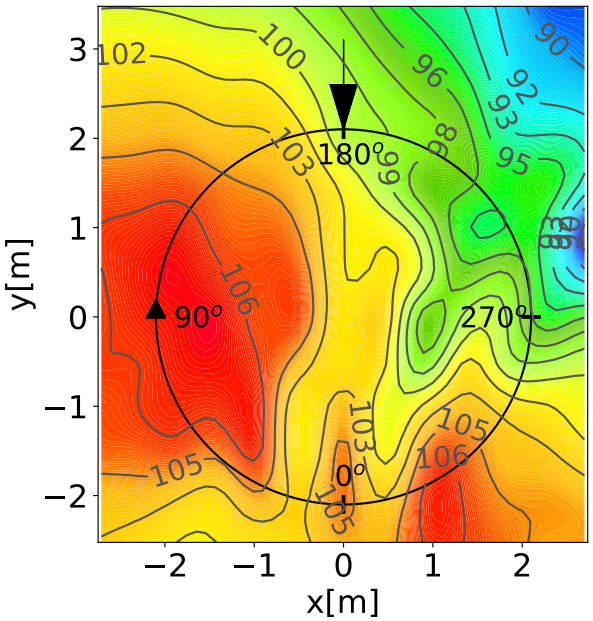

(a) SPL [dB]

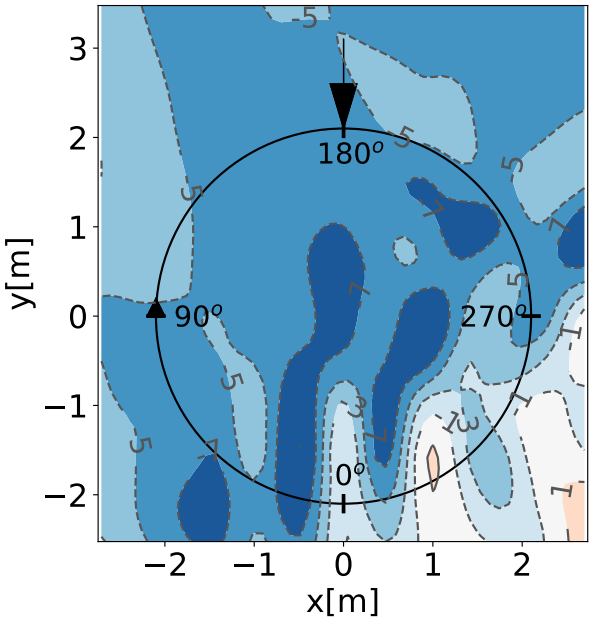

(b) ΔSPL [dB]

Fig. 26: **Coupled UPM** anhedral study - noise and delta noise carpets with

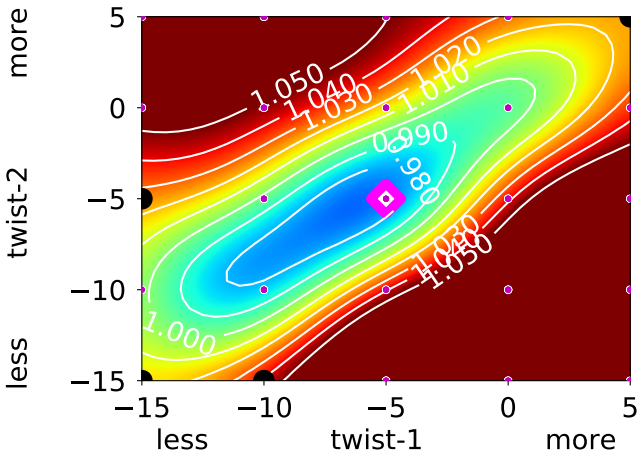

(a) parameter landscape

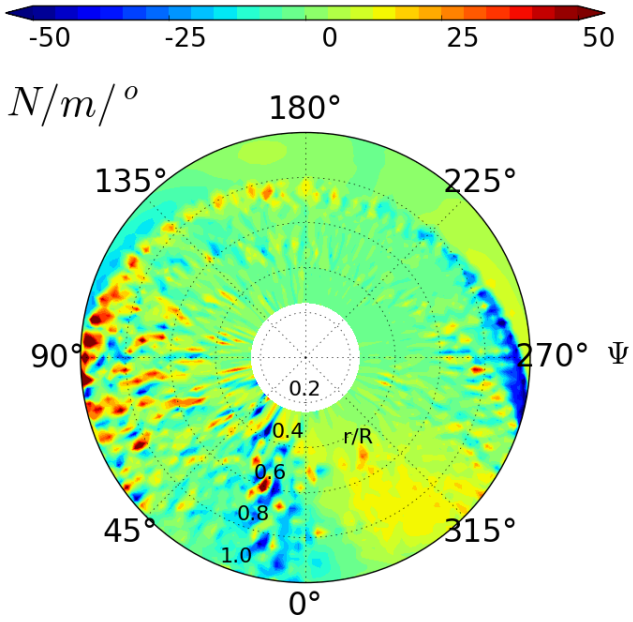

(b) airloads derivatives

Fig. 27: **P.WAKE** twist study - results

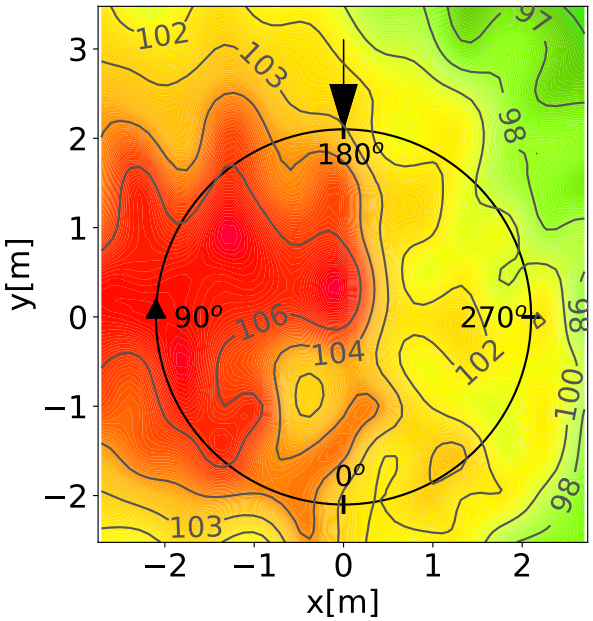

(a) SPL [dB]

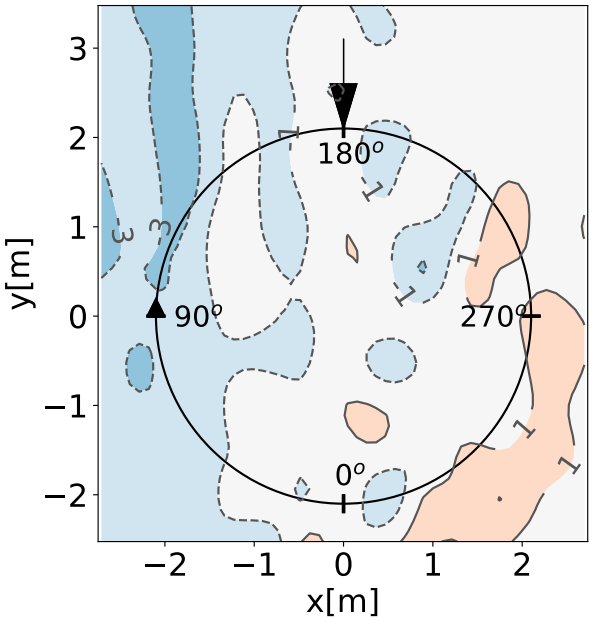

(b) ΔSPL [dB]

Fig. 28: **P.WAKE** twist study - noise and delta noise carpets with

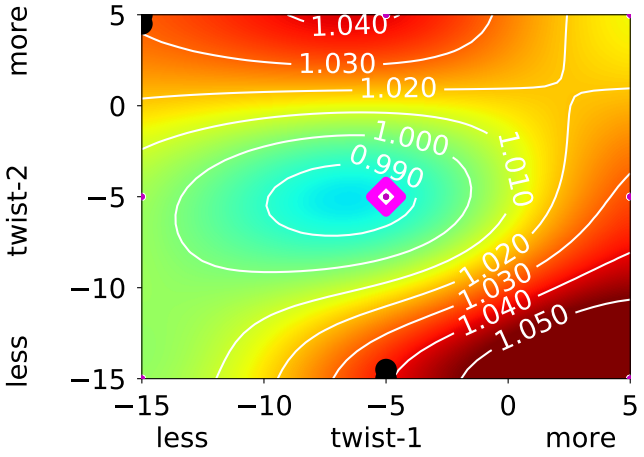

(a) parameter landscape

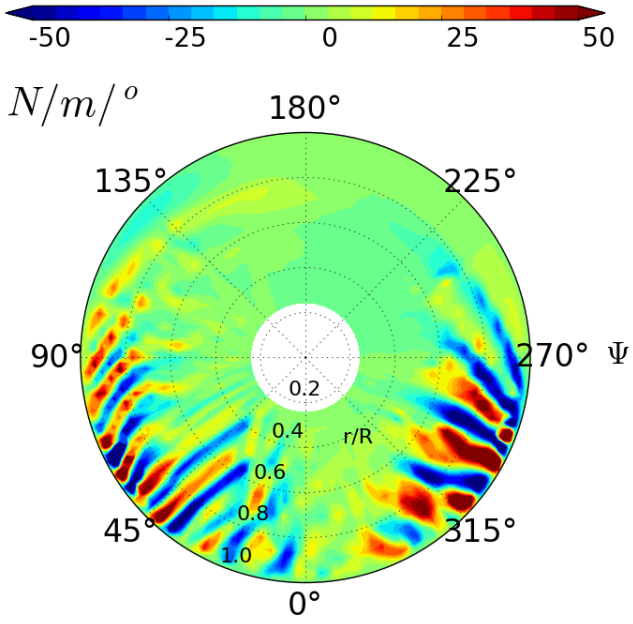

(b) airloads derivatives

Fig. 29: **Coupled UPM** twist study - results

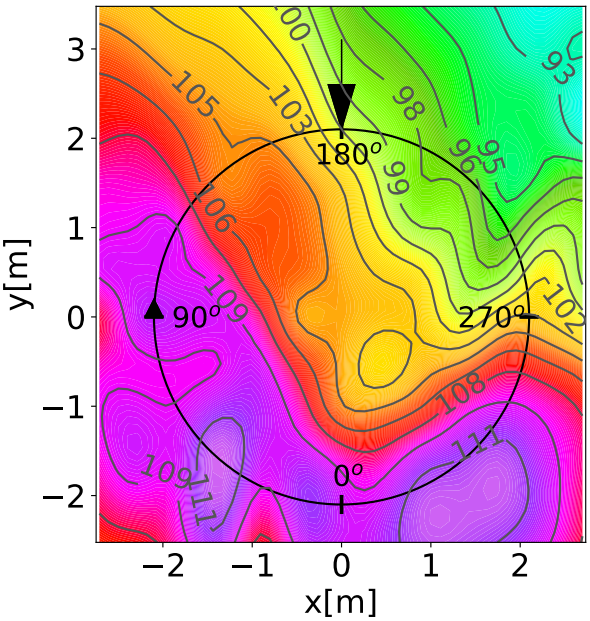

(a) SPL [dB]

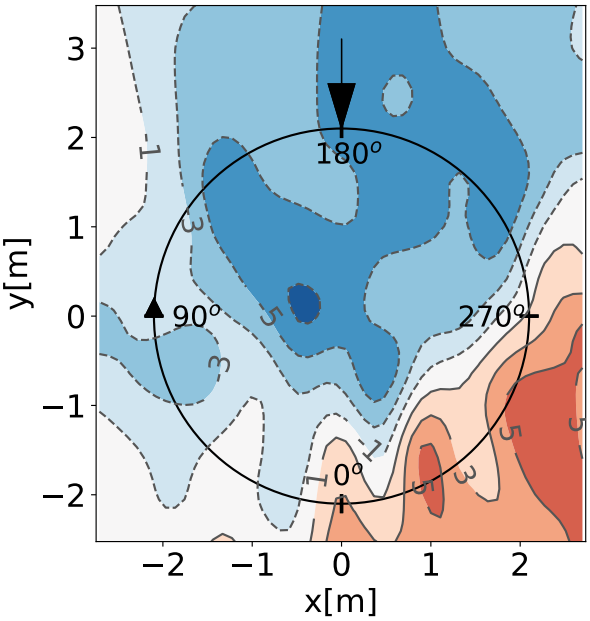

(b) ΔSPL [dB]

Fig. 30: **Coupled UPM** twist study - noise and delta noise carpets with